ELSEVIER

Journal of Organometallic Chemistry 637–639 (2001) 107–115

Journal of Organometallic Chemistry

www.elsevier.com/locate/jorganchem

Conformational control of intramolecular arene stacking in ferrocene complexes bearing *tert*-butyl and pentafluorophenyl substituents

Paul A. Deck [a,*], Caleb E. Kroll [b,1], W. Gary Hollis Jr. [b], Frank R. Fronczek [c]

[a] *Department of Chemistry, Virginia Tech, Blacksburg, VA 24061-0212, USA*
[b] *Department of Chemistry, Roanoke College, Salem, VA 24153, USA*
[c] *Department of Chemistry, Louisiana State University, Baton Rouge, LA 70803-1804, USA*

Received 13 November 2000; received in revised form 20 December 2000; accepted 27 December 2000

Abstract

The reaction of sodium *tert*-butylcyclopentadienide with C_6F_6 and NaH in THF affords either 1-pentafluorophenyl-3-*tert*-butylcyclopentadiene (**1**, as a mixture of double-bond regioisomers) or 1,2-bis(pentafluorophenyl)-4-*tert*-butylcyclopentadiene (**2**), depending on the reaction conditions. Treatment of **1** with NaH in THF affords sodium 1-pentafluorophenyl-3-*tert*-butylcyclopentadienide (**3**). Treatment of **2** with NaH in THF affords sodium 1,2-bis(pentafluorophenyl)-4-*tert*-butyl-cyclopentadienide (**4**). The reaction of the monoarylated ligand (**3**, two equivalents) with $FeBr_2$ in THF affords 1,1′-bis(pentafluorophenyl)-3,3′-di-*tert*-butylferrocene as two diastereomers (*meso*-**5** and *rac*-**5**), which were separated by fractional crystallization from hexane. The X-ray crystal structure of *rac*-**5** reveals a conformation in which the two opposing *tert*-butyl substituents are splayed, enabling transannular stacking of the C_6F_5 groups. In *meso*-**5**, steric repulsion of the two *tert*-butyl substituents prevents intramolecular arene stacking. The reaction of the diarylated ligand (**4**, two equivalents) with $FeBr_2$ in THF affords 1,1′,2,2′-tetrakis(pentafluorophenyl)-4,4′-di-*tert*-butylferrocene (**6**). The crystal structure of **6** reveals no arene stacking. Variable-temperature NMR studies showed that the Cp–Fe–Cp torsional barrier ($\Delta H^{\ddagger}$) of **6** is 17(1) kcal mol^{-1} in dichloromethane-d_2 solution.

Keywords: Crystal engineering; Arene stacking; Ferrocene; Pentafluorophenyl; Conformational analysis

1. Introduction

Arene stacking is a persistent theme in the solid-state structures of metallocenes and other cyclopentadienyl (Cp) complexes bearing pentafluorophenyl (C_6F_5) substituents [1,2]. Hughes and co-workers have rationalized intramolecular arene stacking in the crystal structures of 1,1′-diarylferrocenes (aryl = phenyl, pentafluorophenyl, or one of each) in terms of fundamental crystal engineering concepts [3]. As a part of our continuing study of the synthesis and reactivity of C_6F_5-substituted Cp complexes [4], we aim to explore the possibility of controlling arene stacking through rational structural modification of organometallic complexes.

In this report, we show that a bulky *tert*-butyl (*t*-Bu) group on cyclopentadiene effects complete regiocontrol over the subsequent attachment of one or two C_6F_5 groups. We then describe the synthesis of ferrocenes in which each Cp ligand bears one *t*-Bu group and one or two C_6F_5 groups. We then show, using crystallographic data, how transannular steric interactions of the *t*-Bu groups either enable or prohibit Cp–Fe–Cp conformations in which arene stacking can occur, depending on their stereochemical arrangement. We also compare the enthalpy of activation for Cp–Fe–Cp torsion of 1,1′,2,2′-tetrakis(pentafluorophenyl)-4,4′-di-*tert*-butylferrocene (**6**) with two related complexes, 1,1′,2,2′,4,4′-hexakis(pentafluorophenyl)ferrocene or 1,1′,2,2′,4,4′-hexa(*tert*-butyl)ferrocene.

* Corresponding author. Tel.: +1-540-231-3493; fax: +1-540-231-3255.
E-mail address: pdeck@vt.edu (P.A. Deck).
[1] Undergraduate research participant.

0022-328X/01/$ - see front matter
PII: S0022-328X(01)00878-6

2. Experimental

2.1. General procedures

Standard inert-atmosphere techniques were used for all reactions [5]. Hexafluorobenzene was used as received from Oakwood. Sodium *tert*-butylcyclopentadienide and potassium *tert*-butylcyclopentadienide were prepared from *tert*-butylcyclopentadiene (Aldrich, freshly distilled prior to use) and NaH or KH, respectively, in THF. NMR experiments were performed using JEOL ECP500 and Varian U400 instruments. Dynamic NMR measurements were carried out on the Varian U400, and the temperature scale was calibrated using a MeOH standard. THF-d_8 was vapor-transferred into resealable NMR tubes from Na–K alloy. ^{19}F-NMR spectra were referenced to external C_6F_6 in $CDCl_3$ at -163.00 ppm. $\{^{19}F\}^{13}$C-NMR spectra were particularly useful for resolving signals in the aromatic C–F regions where extensive $^{19}F-^{13}C$ couplings in the ^{1}H-decoupled spectra prevented us from distinguishing closely spaced signals. Furthermore, ^{19}F decoupling provides substantial NOE enhancement of signals that are ordinarily weak under the usual conditions of broadband ^{1}H decoupling. C–F coupling constants were approximated from observed splittings in the $\{^1H\}^{13}$C-NMR spectra. Elemental analyses were performed by Desert Analytics (Tucson, AZ).

2.2. 1-(Pentafluorophenyl)-3-tert-butylcyclopentadiene (1)

A mixture of sodium *tert*-butylcyclopentadienide (1.44 g, 10.0 mmol), hexafluorobenzene (3.72 g, 20.0 mmol), sodium hydride (0.48 g, 20 mmol) and THF (100 ml) was stirred at 25 °C for 20 h. After removing the solvent, hexane (100 ml) and water (50 ml, dropwise at first) were added to hydrolyze the mixture. The biphasic mixture was filtered through Celite and then separated. The aqueous layer was extracted with 25 ml of hexanes. The combined organic layers were washed with water, dried over anhydrous magnesium sulfate, filtered, and evaporated to afford 1.85 g of a brown oil. TLC analysis (silica gel, 250 μm, hexanes) of the oil showed two major products: compound **1** at $R_f = 0.57$ and compound **2** at $R_f = 0.47$. The crude oil was subjected to flash chromatography on silica gel (40×4 cm^2 column), eluting with hexanes to afford 1.02 g (3.54 mmol, 35%) of pure **1** as a colorless oil. A subsequent fraction afforded 160 mg (0.4 mmol, 4%) of pure **2**. Spectroscopic analysis showed that **1** is obtained as a mixture of three double-bond regioisomers (**1a**, 53%; **1b**, 33%; and **1c**, 14%). Assignments are tentative. ^{1}H-NMR ($CDCl_3$): δ **1a**, 7.24 (m, 1H), 6.20 (m, 1H), 3.48 (s, 2H), 1.22 (s, 9H); **1b**, 7.08 (m, 1H), 6.30 (m, 1H), 3.47 (s, 2H), 1.24 (s, 9H); **1c**, 6.66 (m, 1H), 6.39 (m, 1H), 3.17 (s, 2H), 1.23 (s, 9H). ^{19}F-NMR ($CDCl_3$): δ **1a**, -141.26 (m, 2F), -159.08 (t, 1F, $^3J = 21$ Hz), -163.86 (m, 2F); **1b**, -141.75 (m, 2F), -159.77 (t, 1F, $^3J = 21$ Hz), -164.02 (m, 2F); **1c**, -141.38 (m, 2F), -157.65 (t, 1F, $^3J = 21$ Hz), -163.52 (m, 2F). Anal. Found: C, 62.24; H, 4.37. Calc. for $C_{15}H_{13}F_5$: C, 62.50; H, 4.55%.

2.3. 1,2-Bis(pentafluorophenyl)-4-tert-butylcyclopentadiene (2)

A mixture of potassium *tert*-butylcyclopentadienide (3.20 g, 20.0 mmol), hexafluorobenzene (17.0 g, 91.4 mmol), sodium hydride (2.4 g, 0.10 mol) and THF (100 ml) was stirred at 65 °C for 60 h. After removing the solvent, hexane (100 ml) and water (50 ml, dropwise at first) were added to hydrolyze the mixture. The biphasic mixture was filtered through Celite and then separated. The aqueous layer was extracted with 25 ml of hexanes. The combined organic layers were washed with water, dried over anhydrous magnesium sulfate, filtered, and evaporated to afford 6.07 g of a yellow oil. The crude oil was subjected to flash chromatography on silica gel (40×7 cm^2), eluting with hexanes to afford first 230 mg (0.80 mmol, 4%) of **1**, and then 4.44 g (9.8 mmol, 49%) of pure **2**. Because **2** is initially formed as a viscous oil that retains solvent, we waited until the oil spontaneously crystallized (several hours) and then sublimed a small portion (0.05 Torr, 80 °C) to obtain an analytical sample. ^{1}H-NMR ($CDCl_3$): δ 6.29 (s, 1H), 3.54 (s, 2H), 1.26 (s, 9H). ^{19}F-NMR ($CDCl_3$): δ -140.42 (m, 2F), -141.10 (m, 2F), -154.68 (t, 1F, $^3J = 21$ Hz), -155.36 (t, 1F, $^3J = 21$ Hz), -162.01 (m, 2F), -162.16 (m, 2F). $\{^1H\}^{13}$C-NMR ($CDCl_3$): δ 163.0 (s, *C*-*t*-Bu), 133.3 (s, *C*-C_6F_5), 129.0 (t, *C*-C_6F_5, $^3J_{CF} = 2$ Hz), 126.0 (s, CH), 44.1 (t, CH_2, $^4J_{CF} = 2$ Hz), 33.6 (s, CMe_3), 30.6 (s, CH_3). $\{^{19}F\}^{13}$C-NMR ($CDCl_3$): δ 143.9 (s, CF), 143.8 (s, CF), 140.8 (s, CF), 140.3 (s, CF), 137.76 (s, CF), 137.72 (s, CF), 111.6 (s, C_6F_5 *ipso*), 111.2 (s, C_6F_5 *ipso*), 44.1 (td, CH_2, $^1J_{CH} = 127$ Hz, $^4J_{CH} = 9$ Hz), 30.6 (q, CH_3, $^1J_{CH} = 126$ Hz). Anal. Found: C, 55.47; H, 2.33. Calc. for $C_{21}H_{12}F_{10}$: C, 55.52; H, 2.66%.

2.4. Sodium 1-pentafluorophenyl-3-tert-butylcyclopentadienide (3)

A mixture of **1** (1.02 g, 3.54 mmol), sodium hydride (127 mg, 5.31 mmol), and THF (50 ml) was stirred at 25 °C for 15 h. The dark mixture was filtered, the solvent was evaporated, and then most of the residual THF was removed by heating the crude product at 60 °C under a high vacuum (6×10^{-6} mm) for 6 h to afford a dark, sticky solid as the sole product in approximately quantitative yield. ^{1}H-NMR (THF-d_8): δ 6.35 (m, 2H), 5.89 (m, 1H), 1.27 (s, 9H). ^{19}F-NMR (THF-d_8): δ -146.12 (m, 2F), -167.79 (m, 2F), $-$

174.92 (tt, 1F, $^3J = 2$ Hz, $^4J = 6$ Hz). $\{^1H\}^{13}C$-NMR (THF-d_8): δ 108.2 (t, CH, $^4J_{CF} = 8$ Hz), 105.3 (t, CH, $^5J = 3$ Hz), 104.7 (t, CH, $^4J_{CF} = 8$ Hz), 33.4 (s, CH_3), 32.6 (s, CMe_3). Satisfactory microanalytical data were not obtained. ^1H- and ^{19}F-NMR spectra (Figs. S1 and S2) are available from the corresponding author as evidence of substantial purity.

2.5. Sodium 1,2-bis(pentafluorophenyl)-4-tert-butyl-cyclopentadiene (4)

A mixture of **2** (3.37 g, 7.42 mmol), sodium hydride (0.27 g, 11 mmol), and THF (100 ml) was stirred at 25 °C for 15 h. The resulting dark mixture was filtered, the filtrate was evaporated, and the residual THF was removed by heating the crude product at 80 °C under a high vacuum (6×10^{-6} mm) for 12 h to afford a gray solid (quantitative). ^1H-NMR (THF-d_8): δ 6.08 (s, 2H), 1.29 (s, 9H). ^{19}F-NMR (THF-d_8): δ −146.81 (m, 4H), −168.78 (m, 4H), −170.81 (tt, 2H, $^3J = 21$ Hz, $^4J = 2$ Hz). $\{^1H\}^{13}C$-NMR (THF-d_8): δ 144.2 (d, CF, $^1J_{CF} = 252$ Hz), 138.4 (d, CF, $^1J_{CF} = 248$ Hz), 136.2 (d, CF, $^1J = 242$ Hz), 136.2 (s, *C*-C_6F_5), 120.4 (t, C_6F_5 *ipso*, $^2J_{CF} = 19$ Hz), 109.3 (s, CH), 101.2 (s, *C*-*t*-Bu), 33.3 (s, CH_3), 32.4 (CMe_3). $\{^{19}F\}^{13}C$-NMR (THF-d_8): δ 144.2 (s, CF), 138.4 (s, CF), 136.2 (s, CF), 120.4 (s, C_6F_5 *ipso*), 109.3 (dd, CH, $^1J_{CH} = 156$ Hz, $^4J_{CH} = 8$ Hz), 101.2 (t, *C*-*t*-Bu, $^2J_{CH} = 7$ Hz), 33.3 (q, CH_3, $^1J_{CH} = 126$ Hz), 32.4 (s, CMe_3). Satisfactory microanalytical data were not obtained. ^1H- and ^{19}F-NMR spectra (Figs. S3 and S4) are available from the corresponding author as evidence of substantial purity.

2.6. 1,1′-Bis(pentafluorophenyl)-3,3′-di-tert-butylferrocene (5)

A solution of **3** (3.54 mmol) and iron(II) bromide (350 mg, 1.60 mmol) in THF (100 ml) was stirred at 25 °C for 6 h. The solvent was evaporated to afford a dark residue. Benzene (75 ml) and water (25 ml) were added, and the biphasic mixture was filtered through Celite, which was rinsed with 100 ml of hexanes. The biphasic mixture was then separated, and the aqueous layer was extracted with 20 ml of hexanes. The combined organic layers were washed with brine (3×20 ml), dried over anhydrous magnesium sulfate, filtered, and evaporated to afford 0.98 g (1.56 mmol, 97%) of a red–orange crystalline solid. TLC analysis (silica, 250 μm, hexanes) showed a single red spot ($R_f = 0.35$) and traces of the hydrolyzed ligand (**1**, $R_f = 0.57$), suggesting that *meso*-**5** and *rac*-**5** could not be separated by flash chromatography. Instead, the crude product (**5**) was fractionally crystallized from about 10 ml of hexanes, reducing the mother liquors by half for each successive crop. The first crop afforded 190 mg (0.30 mmol, 19%) of pure *meso*-**5**, while the second crop afforded 132 mg (0.21 mmol, 13%) of pure *rac*-**5**. In an alternating fashion, further crops enabled the recovery of additional small amounts of each isomer. Purity for each compound was confirmed by ^1H- and ^{19}F-NMR, while the structural assignments were confirmed by single-crystal X-ray diffraction.

Data for *meso*-**5**: ^1H-NMR ($CDCl_3$): δ 4.43 (m, 2H), 4.40 (m, 2H), 4.38 (m, 2H), 1.19 (s, 18H). ^{19}F-NMR ($CDCl_3$): δ −140.35 (m, 4F), −158.41 (t, 2F, $^3J = 21$ Hz), −163.44 (m, 4F). $\{^1H\}^{13}C$-NMR ($CDCl_3$): δ 104.4 (s, *C*-C_6F_5), 71.8 (s, *C*-*t*-Bu), 71.5 (t, CH, $^4J_{CF} = 5$ Hz), 68.7 (s, CH), 68.3 (t, CH, $^4J_{CF} = 6$ Hz), 31.4 (s, CH_3), 30.6 (s, CMe_3). $\{^{19}F\}^{13}C$-NMR ($CDCl_3$): δ 144.4 (s, CF), 138.7 (s, CF), 138.0 (s, CF), 114.5 (C_6F_5 *ipso*). Anal. Found: C, 57.35; H, 3.82. Calc. for $C_{30}H_{24}F_{10}Fe$: C, 57.16; H, 3.84%.

Data for *rac*-**5**: ^1H-NMR ($CDCl_3$): δ 4.90 (m, 2H), 4.68 (m, 2H), 4.24 (m, 2H). ^{19}F-NMR ($CDCl_3$): δ −139.68 (m, 4F), −159.2 (t, 2F, $^3J = 21$ Hz), −163.88 (m, 4F). $\{^1H\}^{13}C$-NMR ($CDCl_3$): δ 104.8 (s, *C*-C_6F_5), 71.7 (s, *C*-*t*-Bu), 70.4 (t, CH, $^4J_{CF} = 6$ Hz), 68.6 (s, CH), 67.6 (t, CH, $^4J_{CF} = 7$ Hz), 31.5 (s, CH_3), 30.7 (s, CMe_3). $\{^{19}F\}^{13}C$-NMR ($CDCl_3$): δ 144.1 (s, CF), 138.4 (s, CF), 137.6 (s, CF), 112.7 (C_6F_5 *ipso*). Anal. Found: C, 57.09; H, 3.68. Calc. for $C_{30}H_{24}F_{10}Fe$: C, 57.16; H, 3.84%.

2.7. 1,1′,2,2′-Tetrakis(pentafluorophenyl)-4,4′-di-tert-butylferrocene (6)

A solution of **4** (3.40 g, 7.14 mmol) and $FeBr_2$ (721 mg, 3.34 mmol) in THF (100 ml) was stirred at 25 °C for 24 h. The solvent was evaporated to afford a red residue. The residue was dissolved in 100 ml of benzene and filtered through a bed of neutral alumina (30×10 mm^2), using 100 ml of hexanes to elute all of the red product. The dark red filtrate was evaporated to afford a red crystalline solid, which was rinsed with pentane (2×5 ml) and dried under vacuum to afford 3.20 g (3.32 mmol, 98%) of a dark red solid. An analytical sample was obtained by recrystallization from hexanes. ^1H-NMR (CD_2Cl_2, 295 K): δ 4.86 (br s, 2H), 4.78 (br s, 2H), 1.11 (s, 18H). ^{19}F-NMR (CD_2Cl_2, 295 K): δ −139.89 (br, 4F), −140.64 (m, 4F), −159.30 (t, 2F, $^3J_{FF} = 21$ Hz), −160.28 (t, 2F, $^3J = 21$ Hz), −166.70 (m, 4F), −167.97 (m, 4F). Anal. Found: C, 52.04; H, 2.23. Calc. for $C_{42}H_{22}F_{20}Fe$: C, 52.41; H, 2.30%.

2.8. Crystallography

Crystals of *meso*-**5** and *rac*-**5** were obtained by cooling concentrated hexanes solutions to −5 °C for 24 h. Crystals of **6** obtained from hexanes revealed disordered solvent molecules that were difficult to model. Superior crystals were obtained by cooling a concentrated $CDCl_3$ solution of **6** to −5 °C for 2 days.

Relevant crystal data are assembled in Table 1. Details of the crystallographic experiments as well as complete tables of metric parameters are available from the corresponding author.

3. Results and discussion

3.1. Ligand synthesis

We showed earlier that Cp anions react with perfluoroarenes in nucleophilic aromatic substitution reactions to afford fluoroarylated cyclopentadienes [4]. In the present study, we started with *tert*-butylcyclopentadiene in order to examine the effect of the bulky *t*-Bu group on the regioselectivity of this process. Scheme 1 shows that this reaction procedes with complete regioselectivity for arylation distal to the *tert*-butyl group. The ^{1}H- and ^{19}F-NMR spectra of the crude monoarylation product (**1**) revealed the presence of three distal double-bond regioisomers in a ratio of about 5:3:1. Additional isomers would require either (a) attaching the aryl group proximal to the *t*-Bu group, which is apparently prohibited by steric congestion in the nucleophilic aromatic substitution transition state, or (b) placing the aryl group, the *t*-Bu group, or both on the sp^3-hybridized carbon atom of the cyclopentadiene. Moving the aryl group to the sp^3-hybridized position would disrupt conjugation, while moving the *t*-Bu group to the sp^3-hybridized position would violate Saytzeff's rule. Regarding the precise spectral assignments, we were unable to further distinguish unambiguously which ^{1}H- and ^{19}F-NMR spectra signals corresponded to each of the three isomers. Selectivity for monoarylation or diarylation is achieved by varying the reaction conditions. At 25 °C (20–40 h), the monoarylated cyclopentadiene (**1**) is the major product, whereas a longer reaction (60 h) at 65 °C affords nearly pure diarylated product (**2**), both in moderate yields. The two products (**1** and **2**) are readily separated and purified by silica gel chromatography. For the reasons outlined above, the diarylated cyclopentadiene (**2**) is obtained as a single regioisomer.

As shown in Scheme 1, both of the dienes (**1** and **2**) are readily converted to the corresponding sodium salts in essentially quantitative yields. Formation of a single

Table 1
Crystallographic data

Compound	*meso*-**5**	*rac*-**5**	**6**
Empirical formula	$C_{30}H_{24}F_{10}Fe$	$C_{30}H_{24}F_{10}Fe$	$C_{42}H_{22}F_{20}Fe{\cdot}CDCl_3$
Formula weight	630.34	630.34	1081.81
Diffractometer	Nonius Kappa CCD	Nonius Kappa CCD	Nonius Kappa CCD
Crystal size (mm)	$0.28\times0.27\times0.12$	$0.35\times0.25\times0.22$	$0.35\times0.25\times0.08$
Crystal system	Monoclinic	Monoclinic	Triclinic
Unit cell dimensions			
a (Å)	10.0450(3)	14.5540(3)	11.1680(2)
b (Å)	8.9440(2)	12.6950(4)	20.0280(6)
c (Å)	29.5860(8)	14.4570(4)	20.2450(6)
α (°)			70.8390(12)
β (°)	91.0590(14)	95.6590(17)	80.4250(17)
γ (°)			81.9660(18)
V (Å^3)	2657.63(12)	2658.10(12)	4200.1(2)
Space group	$P2_1/c$ (no. 14)	$P2_1/c$ (no. 14)	$P\bar{1}$ (no. 2)
Z	4	4	4
D_{calc} (Mg m^{-3})	1.575	1.575	1.711
Absorption coefficient (mm^{-1})	0.7	0.7	0.7
$F(000)$	1280	1280	2152
λ (Mo–K$_\alpha$) (Å)	0.71073	0.71073	0.71073
Temperature (K)	120	120	120
Theta range for data collection (°)	2.7–32.0	2.6–30.0	2.5–30.0
No. of reflections collected	21967	12876	43374
No. of independent reflections	9125	7739	24072
Absorption correction method	Multi-scan	Multi-scan	Multi-scan
Max/min transmission	0.925, 0.806	0.869, 0.832	0.948, 0.828
H treatment	Constrained	Constrained	Constrained
Data/restraints/parameters	9125/0/376	7739/0/376	24072/0/1219
R [$I>2$ and (I)]	0.034	0.035	0.053
R_w [$I>2$ and (I)]	0.080	0.096	0.142
Goodness-of-fit on F^2	0.89	1.02	0.92
Largest difference peak and hole (e Å^{-3})	0.43 and −0.40	0.32 and −0.38	1.03 and −1.14

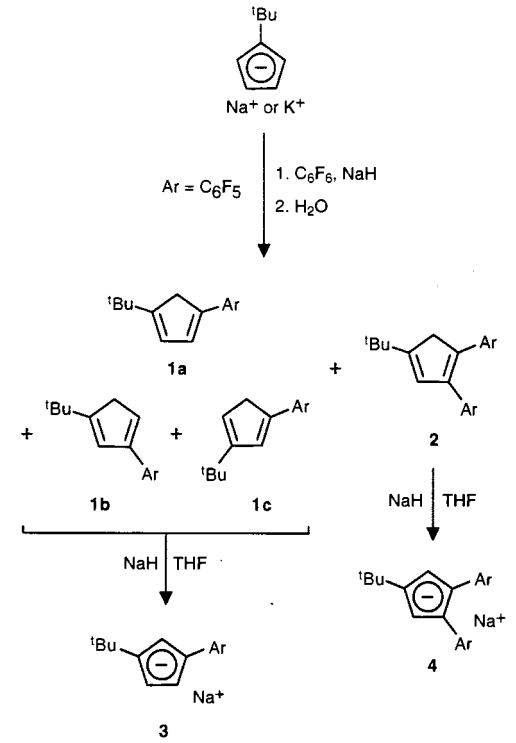

Scheme 1.

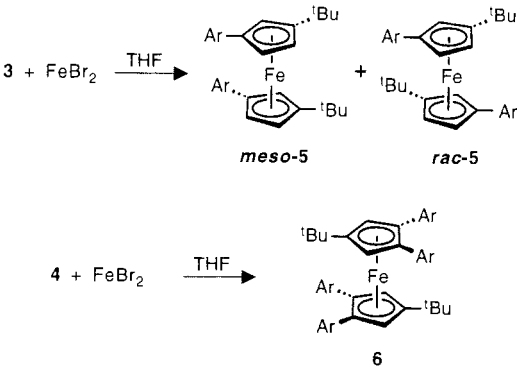

Scheme 2.

Cp anion from the monoarylated diene (**1**) supports the assignment of a single regiochemical relationship between the *t*-Bu and C_6F_5 groups. Both sodium salts (**3** and **4**) are thermally stable (to at least 100 °C) but air-sensitive. ^{13}C-NMR analysis of the monoarylated anion (**3**) provides evidence of the distal regiochemistry (Chart 1). The three signals assigned to the methine (CH) carbons at 108.2, 105.3, and 104.7 ppm exhibit long-range C–F couplings of 8, 3, and 8 Hz, respectively. In the observed distal regioisomer, two CH carbons would exhibit the larger four-bond coupling constant (8 Hz), and one CH carbon would exhibit a smaller five-bond coupling constant (3 Hz), whereas in the proximal regioisomer, two smaller coupling constant and one larger coupling constant would be expected. This regiochemical assignment was ultimately confirmed by crystallographic analysis of the corresponding ferrocene derivatives.

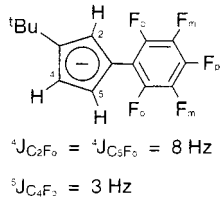

Chart (1)

3.2. Metallocene synthesis

The arylated ligands (**3** and **4**) reacted smoothly with $FeBr_2$ in THF (Scheme 2) to afford high yields of the corresponding ferrocene complexes (**5** and **6**). The monoarylated ligand (**3**) afforded a roughly 1:1 mixture of *meso*-**5** and *rac*-**5**. By careful fractional crystallization from hexanes, we isolated pure *meso*-**5** from the first, third, and fifth crops of crystals. The second and fourth crops contained mostly *rac*-**5**. Purities of individual crops were established by ^{1}H- and ^{19}F-NMR spectroscopy, and individual well-formed crystals were selected for crystallographic analysis (see below). Both complexes are crystalline solids having the dark orange color that is typical of ferrocene complexes. The tetraarylated ferrocene (**6**) was isolated as a deep red crystalline solid. All three complexes (*meso*-**5**, *rac*-**5**, and **6**) are air-stable and were fully characterized by ^{1}H-, ^{19}F-, and ^{13}C-NMR spectroscopy as well as elemental microanalysis and single-crystal X-ray diffraction (see below).

3.3. Structural studies

The molecular structure of *meso*-**5** is shown in Fig. 1a. Selected metric data are provided in Table 2. Noteworthy is the absence of intramolecular arene stacking (Fig. 1b). A survey of prior studies of 1,1′-bis(pentafluorophenyl)-substituted ferrocene complexes (e.g. **7**–**9**) reveal that the structure in which the two C_6F_5 groups are engaged in π-stacking is the solid-state conformational minimum. However, based on Okuda's earlier investigations of Cp–Fe–Cp conformational dynamics in *t*-Bu-substituted ferrocenes, we also know that the transannular steric interaction of two *t*-Bu groups in either eclipsing [$\alpha \equiv \angle$(*t*-Bu–Cp–Cp′–*t*-Bu′) = 0°] or even *gauche* ($\alpha = 36°$) conformations is strongly avoided [9]. These interactions prevent *meso*-**5** from adopting a conformation ($\alpha \approx 0°$) that would enable stacking of the two C_6F_5 groups. The actual conformation is defined by $\alpha = 82.5°$.

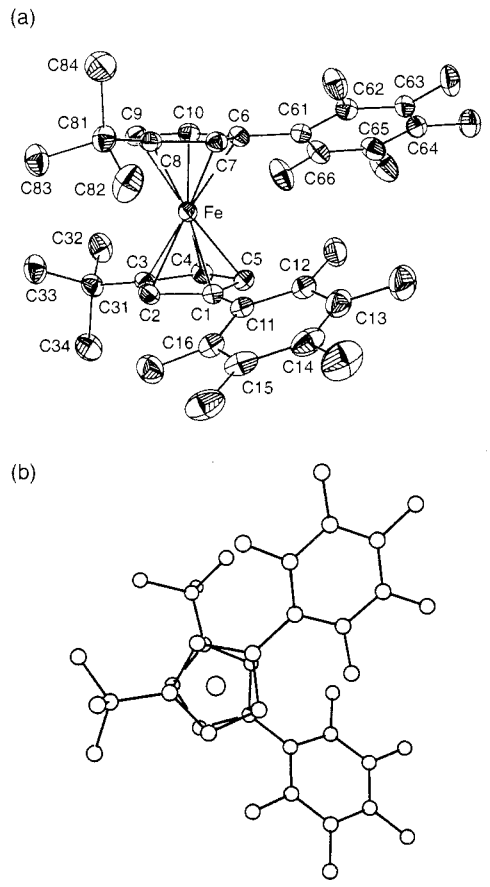

Fig. 1. Crystal structure of *meso*-**5**. (a) Thermal ellipsoid plot shown at 50% probability. H atoms were removed for clarity. F atoms are numbered as the attached C atoms. (b) Ball-and-stick diagram showing Cp–Fe–Cp conformation.

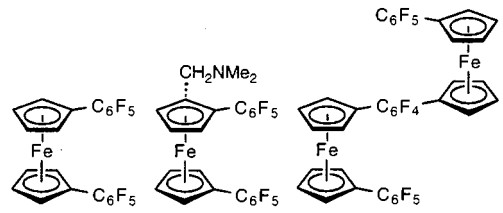

The molecular structure of *rac*-**5** (Fig. 2, Table 2) supports this analysis. In *rac*-**5**, stacking of the two C_6F_5 groups (Fig. 2b) can be achieved without approaching conformational angles in which the two *t*-Bu engage in strong mutual repulsions. The observed conformation is defined by $\alpha = 82.6°$, nearly the same value as observed for *meso*-**5**. Interestingly, the C_6F_5–C_6F_5 stacking motif in *rac*-**5** is 'tighter' than in other related complexes that we have analyzed. For example, the C_6F_5(centroid)–C_6F_5(centroid) distance of 3.39 Å is nearly 0.2 Å shorter than the non-butylated parent compound (**7**), which exhibits a corresponding distance of 3.58 Å [3]. The angle of 4.4° between the two C_6F_5 planes of *rac*-**5** also suggests a well-organized stacking arrangement. Corresponding interplanar angles in other C_6F_5-substituted ferrocenes that we have studied range from 5° to 17° [1,2]. The C_6F_5(centroid)–C_6F_5(least-squares plane) distances (3.225 and 3.271 Å) of *rac*-**5** are less than C_6F_5(centroid)–C_6F_5(centroid) distance because of the tilting of aryl groups relative to their respective Cp ligands by 28 and 26°, respectively. Corresponding Cp–C_6F_5 tilting angles in **7** are both 25° [3].

Table 2
Selected bond lengths (Å) and bond angles (°) for *meso*-**5**, *rac*-**5**, and **6** [a]

	meso-**5**	*rac*-**5**	**6a**	**6b**		*meso*-**5**	*rac*-**5**	**6a**	**6b**
Fe–C1	2.041(1)	2.056(1)	2.091(3)	2.071(3)	Fe–C6	2.043(1)	2.049(1)	2.107(3)	2.111(3)
Fe–C2	2.049(1)	2.049(1)	2.111(3)	2.116(3)	Fe–C7	2.047(1)	2.050(1)	2.076(3)	2.087(3)
Fe–C3	2.083(1)	2.079(1)	2.076(3)	2.077(3)	Fe–C8	2.076(1)	2.080(1)	2.055(3)	2.050(3)
Fe–C4	2.052(1)	2.061(1)	2.107(3)	2.104(3)	Fe–C9	2.054(1)	2.056(1)	2.102(3)	2.103(3)
Fe–C5	2.037(2)	2.037(1)	2.054(3)	2.054(3)	Fe–C10	2.034(1)	2.038(1)	2.074(3)	2.081(3)
Fe–Cp1 [b]	1.655(1)	1.660(1)	1.698(3)	1.695(3)	Fe–Cp2 [b]	1.653(1)	1.659(1)	1.694(3)	1.695(3)
C1–C11	1.479(2)	1.475(2)	1.472(4)	1.490(4)	C6–C61	1.476(2)	1.479(2)	1.476(4)	1.477(4)
C2–C21			1.481(4)	1.478(4)	C7–C71			1.489(4)	1.478(4)
C3–C31	1.522(2)	1.520(2)			C8–C81	1.524(2)	1.519(2)		
C4–C41			1.522(4)	1.518(4)	C9–C91			1.536(4)	1.525(4)
Cp1–Fe–Cp2″	178	180	174	174	α [c]	83	83	100	102
β1 [d]	22	29	39	35	β2 [d]	28	26	45	41
β3 [d]			44	47	β4 [d]			29	32

[a] Crystalline **6** shows two nearly identical molecules per asymmetric unit, designated **6a** and **6b**.
[b] Cp1 and Cp2 are the centroid of C1–C5 and C6–C10, respectively.
[c] α is the torsion angle C(*t*-Bu)–Cp1–Cp2–C(*t*-Bu) (absolute value).
[d] β1–β4 are Cp-aryl interplanar torsion angles (absolute values). β1: (C1–C5)–(C11–C16); β2: (C1–C5)–(C21–C26); β3: (C6–C10)–(C61–C66); and β4: (C6–C10)–(C71–C76).

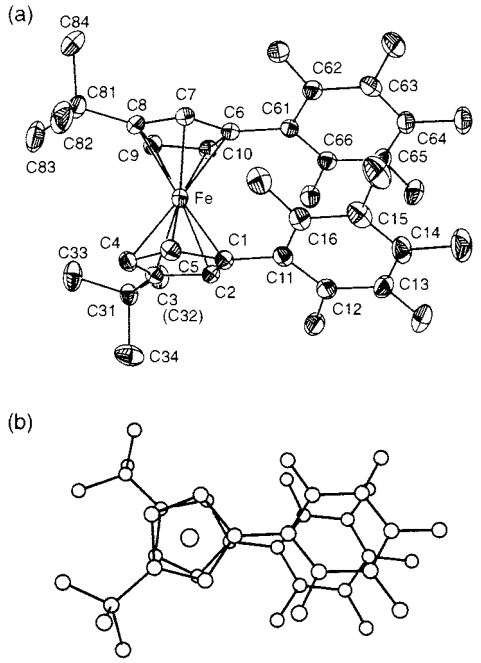

Fig. 2. Crystal structure of *rac*-**5**. (a) Thermal ellipsoid plot shown at 50% probability. H atoms were removed for clarity. F atoms are numbered as the attached C atoms. (b) Ball-and-stick diagram viewed along the Cp–Fe–Cp axis showing transannular arene stacking.

The molecular structure of **6** is shown in Fig. 3a. Rationalizing the observation that **6**·$CDCl_3$ does not engage in intramolecular arene stacking requires closer inspection of transannular interactions (Fig. 3b). The F26–F72 and F16–F66 distances are 2.56 and 2.59, respectively. Turning the 'bottom' ligand to increase the stacking interaction between the C21–C26 and C61–C66 aryl substituents would decrease both of these F–F distances and introduce additional strain. The C16–C66 and C71–C76 aryl groups cannot twist about their Cp–C_6F_5 axes to relieve this strain because of transannular interactions with the *tert*-butyl groups via C44 and C94.

Neither *meso*-**5**, *rac*-**5**, nor **6**·$CDCl_3$ exhibits intermolecular arene stacking. The packing diagram of *meso*-**5** shows a pairwise Cp–C_6F_5 'stacking' motif, but the Cp(centroid)-to-C_6F_5(centroid) distance of 3.828 and the Cp-to-C_6F_5 interplanar angle of 29.4° suggest that this feature of the packing arragement is poorly organized and insignificant.

Additional metric data in Table 2 shows that while *meso*-**5** and *rac*-**5** are relatively unstrained about their metallocene cores, the tetraarylated complex shows a slight 'bend' in the Cp–Fe–Cp angle (visible in Fig. 3a). The Fe–C distances show that none of these complexes exhibits significantly 'slipped' or 'hinged' Cp ligands [6], although the carbon atoms (C3, C8) bearing the *tert*-butyl substituents tend to be more distant from the iron atom in *meso*-**5** and *rac*-**5**. The Cp–C_6F_5 interplanar angles (β1–β4, Table 2) lie in the range 20–50, typical of other C_6F_5-substituted ferrocenes that we have studied [2]. These angles tend to the lower end of this range when additional steric constraints such as those imposed by bulky vicinal substituents are absent, whereas **6** exhibits β angles that are toward the upper end of the typical range. The longer Fe–Cp distances in **6** also suggest that **6** shows transannular steric repulsion, because one would expect the additional electron-withdrawing C_6F_5 groups to decrease Fe–C distances [7].

3.4. Dynamic NMR studies

The NMR spectra of **6** reveal an exchange process described in Fig. 4. The ligand substitution pattern alone suggests time-averaged C_{2h} (**6a**) or C_{2v} (**6f**) symmetry with all four Cp protons and all four C_6F_5 groups chemically equivalent. In fact, Hanusa and coworkers found that [1,2,4-$Cy_3C_5H_2]_2Fe$ (Cy = cyclohexyl) adopts approximate C_{2h} symmetry in the solid state [8]. However, the ^{1}H-NMR spectrum of **6** at 23 °C shows a pair of exchange-broadened signals. At room temperature, the two diastereotopic C_6F_5 groups

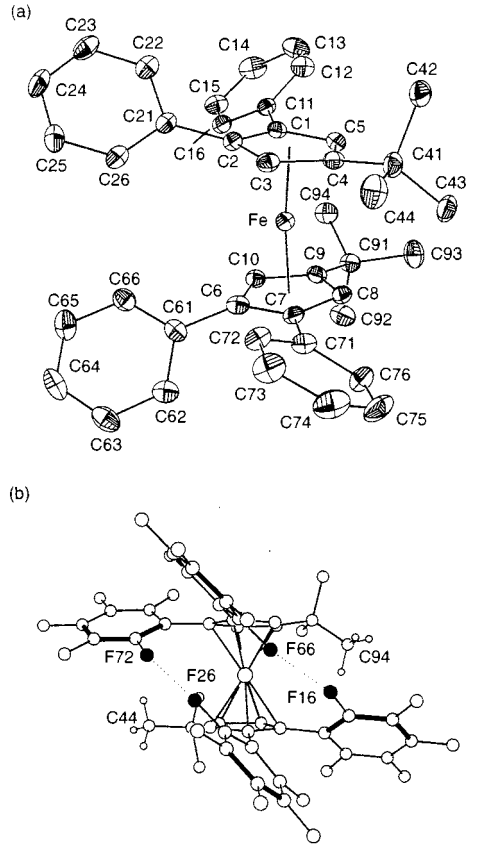

Fig. 3. Crystal structure of **6**·$CDCl_3$. (a) Thermal ellipsoid plot shown at 50% probability. H and F atoms were removed for clarity. (b) Ball-and-stick diagram showing Cp–Fe–Cp conformations. Darkened F and dotted lines atoms indicate transannular F···F repulsions that prevent stacking of the C21–C26 and C61–C66 aryl substituents.

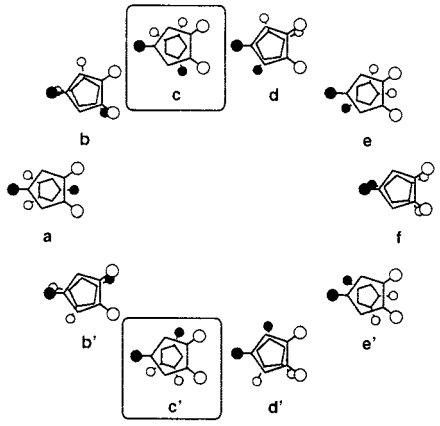

Fig. 4. Conformational analysis of **6**. Boxed diagrams correspond to the crystal structure. Filled circle = *tert*-butyl; open circle = C_6F_5 (Fig. 3).

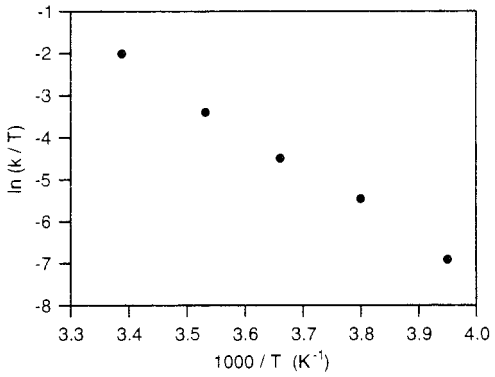

Fig. 5. Eyring plot of rate constants for Cp–Fe–Cp rotation in **6**.

are also in the slow-exchange spectral regime in the ^{19}F-NMR spectrum. Lineshape analyses of the ^{1}H spectrum at several temperatures in the slow-exchange regime (-20 to 22 °C, spectra are available from the corresponding author) and application of Eq. (1) lead to an Eyring plot (Fig. 5), from which we obtain the activation parameters ($\Delta H^{\ddagger} = 17 \pm 2$ kcal mol^{-1}, $\Delta S^{\ddagger} = 6 \pm 6$ e.u., and $\Delta G^{\ddagger}_{298} = 15 \pm 2$ kcal mol^{-1}) for Cp–Fe–Cp rotation in **6**. Notably, this enthalpy of activation is comparable to corresponding values obtained for hexakis(*tert*-butyl)ferrocene (15 kcal mol^{-1}) [9] but slightly higher than that obtained for hexakis(pentafluorophenyl)ferrocene (11 kcal mol^{-1}) [1]. Examination of the crystal structure of **6** (Fig. 3) suggests that this exchange could be represented by the racemization **6c** ⇄ **6c**′ [5], probably proceeding via **6a** to avoid the *t*-Bu–*t*-Bu interaction in **6f**. Estimating the Cp–Fe–Cp and Cp–C_6F_5 rotational barriers was not achieved for *meso*-**5** and *rac*-**5**, because we were unable to observe the slow-exchange regimes of the ^{19}F-NMR spectra even after cooling the samples to -90 °C.

4. Conclusions

A single *tert*-butyl substituent on the Cp anion directs arylation by C_6F_6 to distal positions. Isomeric ferrocene complexes bearing one *t*-Bu and one C_6F_5 group on each Cp ligand exhibit intramolecular arene stacking only if the stacking conformation is consistent with the conformational preferences of opposing *t*-Bu groups.

5. Supplementary material

The following data are available from the corresponding author: NMR data for **3** and **4**, variable-temperature ^{1}H-NMR spectra of **6** and an associated table of rate data.

Crystallographic data for the structural analysis have been deposited with the Cambridge Crystallographic Data Centre, CCDC nos. 154483, 154484, and 154485, for compounds *rac*-**5**, *meso*-**5**, **6**·$CDCl_3$, respectively. Copies of this information may be obtained free of charge from The Director, CCDC, 12 Union Road, Cambridge CB2 1EZ, UK (Fax: +44-1223-336033; e-mail: deposit@ccdc.cam.ac.uk or www: http://www.ccdc.cam.ac.uk).

Acknowledgements

This work was supported in part by a grant from the Jeffress Memorial Trust to W.G.H., a Roanoke College Summer Scholarship to C.E.K., and the Virginia Tech Chemistry Department.

References

[1] (a) M.P. Thornberry, C. Slebodnick, P.A. Deck, F.R. Fronczek, Organometallics 19 (2000) 5352;
(b) M.P. Thornberry, C. Slebodnick, P.A. Deck, F.R. Fronczek, Organometallics 20 (2001) 920.
[2] P.A. Deck, M.J. Lane, J.L. Montgomery, C. Slebodnick, F.R. Fronczek, Organometallics 19 (2000) 1013.
[3] M.D. Blanchard, R.P. Hughes, T.E. Concolino, A.L. Rheingold, Chem. Mater. 12 (2000) 1604.
[4] P.A. Deck, W.F. Jackson, F.R. Fronczek, Organometallics 15 (1996) 5287.
[5] (a) A.B. Pangborn, M.A. Giardello, R.H. Grubbs, R.K. Rosen, F.J. Timmers, Organometallics 15 (1996) 1518;
(b) D.F. Shriver, M.A. Drezdzon, The Manipulation of Air-Sensitive Compounds, Wiley, New York, 1986.
[6] (a) T.B. Marder, J.C. Calabrese, C.D. Roe, T.H. Tulip, Organometallics 6 (1987) 2012;
(b) S.A. Wescott, A.K. Kakkar, G. Stringer, N.J. Taylor, T.B. Marder, J. Organomet. Chem. 394 (1990) 777;
(c) J.W. Faller, R.H. Crabtree, A. Habib, Organometallics 4 (1985) 929;

(d) R.T. Carl, R.P. Hughes, A.L. Rheingold, T.B. Marder, N.J. Taylor, Organometallics 7 (1988) 1613;
(e) R.T. Baker, T.H. Tulip, Organometallics 5 (1986) 839.
[7] P.G. Gassman, C.H. Winter, J. Am. Chem. Soc. 110 (1988) 6130.
[8] J.A. Burman, M.L. Hays, D.J. Burkey, P.S. Tanner, T.P. Hanusa, J. Organomet. Chem. 479 (1994) 135.
[9] (a) J. Okuda, Top. Curr. Chem. 160 (1991) 97;
(b) J. Okuda, E. Herdtweck, Chem. Ber. 121 (1988) 1899;
(c) C. Janiak, H. Schumann, Adv. Organomet. Chem. 33 (1991) 291;
(d) J. Okuda, J. Organomet. Chem. 367 (1989) C1;
(e) E.W. Abel, N.J. Long, K.G. Orrell, A.G. Osborne, V. Šik, J. Organomet. Chem. 403 (1991) 195.